Turbulence analysis from long-exposure-time acquisitions with Interferometric Rayleigh Scattering

T.Castelain[1,*], I.Kurek[2], Pierre Lecomte[1], Christophe Bailly[2]

1: Universite Claude Bernard Lyon 1, Ecole Centrale de Lyon, CNRS, INSA Lyon, LMFA, UMR5509, 69622 Villeurbanne, France;
2: Ecole Centrale de Lyon, CNRS, Universite Claude Bernard Lyon 1, INSA Lyon, LMFA, UMR5509, 69130 Ecully, France
*Corresponding author: thomas.castelain@univ-lyon1.fr

Keywords: Rayleigh scattering, flow velocity, turbulence level.

ABSTRACT

This study focuses on the analysis of long-exposure-time interferograms obtained with an Interferometric Rayleigh Scattering (IRS) set-up pointing at a high subsonic isothermal jet flow. The objectives are twofold : retrieve from seeding-free optical measurements the mean characteristics of this flow - in particular the mean velocity profile in the jet shear-layer - and determine higher order statistics for the flow velocity in the shear layer. The results are compared to those obtained on the same test bench by use of hot wire anemometry, and conclusions about the relevancy of the approach together with potential improvements are deduced therefrom.

1. Introduction

Molecular scattered light, that is light scattered by molecules as incident light of frequency ν_0 is directed towards these molecules, is used to determine the local density (Mercier et al., 2018), velocity and temperature (Seasholtz et al., 1997; Panda & Seasholtz, 1999) in high-speed flows where the use of a probe or seeding may be inappropriate. The spectral characteristics of the scattered light by molecules contain indeed the footprint of molecular motions, which can be viewed as Doppler-Fizeau effects. The molecular agitation in a given volume of molecules at rest, from a macroscopic viewpoint, induces a broadening $\Delta\nu_T$ of the light spectrum, which is large with respect to the bandwidth $\Delta\nu_0$ of the incident light as produced by a fiber laser, as depicted in Figure 1(a). This broadening is described here by use of the Tenti S6 model (Tenti et al., 1974). If the probed volume has a bulk motion, as in the case of gas flow, a shift in frequency $\Delta\nu_U$ of the spectrum superimposes on that obtained for the same volume of molecules at rest, as illustrated in Figure 1(b). In orders of magnitude, if using a light source of wavelength $\lambda_0 = 532$ nm, corresponding to $\nu_0 = 5.64 \times 10^5$ GHz, with a bandwidth $\Delta\nu_0 = 2 \times 10^{-4}$ GHz (which are the characteristics of the laser used hereafter), directed toward an air flow at temperature T=300 K and velocity U=300 m.s^{-1}, the thermal

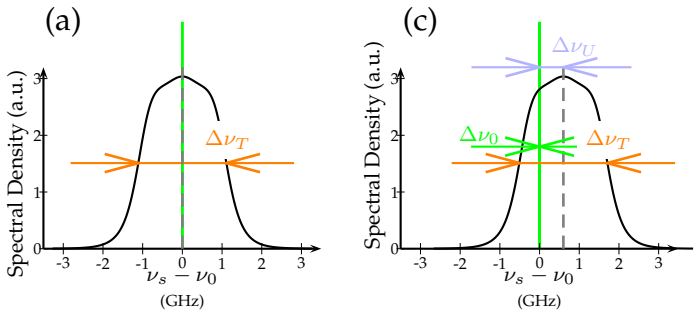

Figure 1. Spectral content of the scattered light by molecules (a) at rest and at temperature $T = 300$K (b) with a bulk motion at velocity $U = 300$ m.s^{-1} and at temperature $T = 300$K

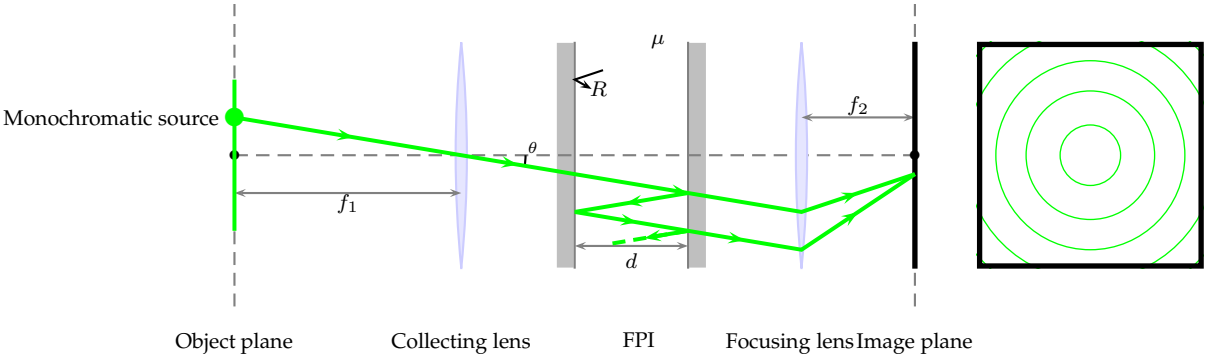

Figure 2. Optical arrangement for interferometric measurements

broadening of the spectrum is evaluated to $\Delta\nu_T = 2.2$ GHz and the frequency shift due to bulk motion $\Delta\nu_U = 0.56$ GHz. The frequency shifts $\Delta\nu_T$ and $\Delta\nu_U$ have thus the same order of magnitude, which is five times lower than that of the light source frequency. The measurement of these spectral quantities requires thus the use of an interferometer, that allows to form interferograms as sketched in Figure 2. In this optical arrangement, an air-spaced Fabry-Pérot Interferometer (FPI), with mirrors of reflectivity R and a spacing d between reflective surfaces, is placed between a focusing lens of focal length f_2 and a collecting lens of focal f_1. The light source, of given spatial extension, is placed in the focal plane of this lens, and a camera sensor is placed in the focal plane of the collecting lens.

Provided that the light source is homogeneous and monochromatic (wavelength λ) in the object plane, the light intensity distribution in the image plane would also be homogeneous if the FPI is removed from the optical arrangement of Figure 2. Let us define I_0 as the light intensity in this case. With the FPI as depicted in Figure 2, the intensity distribution may be approximated with:

$$I_{FP}(\lambda, r) = \frac{I_0}{1 + \left(\frac{2N_R}{\pi}\right)^2 \sin^2\left(\frac{2\pi\mu d}{\lambda}\left(1 - \frac{1}{2}\left(\frac{r}{f_2}\right)^2\right)\right)} \tag{1}$$

with N_R the FPI finesse, μ the optical index of air surrounding the FPI mirrors, and r the radial distance between any point in the image plane and the optical axis. This defines circular bright rings

in the image plane, whose width depends on the FPI finesse. For this reason, the intrinsic characteristics of the FPI, N_R and μd, are usually derived from the analysis of such an interferogram; I_{FP} is thus referred to as the Fabry-Pérot instrument function.

In the case of Rayleigh scattered light, of broadband spectral content $S_R(\lambda)$, superposition principle leads to the intensity distribution under the form:

$$I(r) = \int_{-\infty}^{\infty} S_R(\lambda) I_{FP}(\lambda, r) \mathrm{d}\lambda \tag{2}$$

which defines the light intensity distribution in what will be called Rayleigh interferogram in the following. The rings width results in this case from the FPI finesse and the spectral content of the Rayleigh scattered light. If the FPI finesse is known, the analysis of the rings location and width leads to the determination of the spectral content of the scattered light, thus to the flow speed U and temperature T. For steady flows, the intensity distribution is time independent; the exposure time used for interferogram recordings can be large so that the signal to noise ratio achieves a value reasonably high to perform the data processing in good conditions. In the case of turbulent flows, such as in the shear layer of a high speed jet, significant changes in local temperature and velocity occur at small time scales. To avoid a blurring of the interferogram due to time-integration effects, one should capture interferograms from the light scattered by molecules in these regions with a low exposure time with respect to turbulence time scales, which requires a high-speed imaging system and high-power laser source (Cutler et al., 2020; Estevadeordal et al., 2018), that can also be combined with intensified cameras (Panda, 2020; Estevadeordal et al., 2018). If the exposure time is high with respect to the turbulence time scales, the rings width in the interferogram would result from the unsteady thermal broadening $\Delta\nu_T(t)$ as well as the unsteady frequency shift due to bulk motion $\Delta\nu_U(t)$. The unwrapping from the interferogram analysis between the two effects to recover the true temperature and velocity standard deviations is *a priori* impossible. In the case of an isothermal turbulent flow, the change in temperature at any point is zero. Thus, the width of the rings in the long exposure time interferogram is due to unsteady shifts in frequency, whose occurrence depends on the turbulence spectrum and whose magnitude depends on the turbulence level. Consequently, the analysis of a long exposure time interferogram obtained from the shear layer of an isothermal flow should in principle allow for the characterization of the turbulence in this flow. The aim here is to obtain a turbulence level estimation using Rayleigh scattered light only, which differs from the pioneering approach of Mielke et al. (2005) where Mie scattering has been considered for turbulence measurements. The objective of the present work is to present an experimental investigation of this optical approach and to compare its results to that derived from Constant Temperature Anemometry (CTA) reference measurements.

2. Experimental set-up

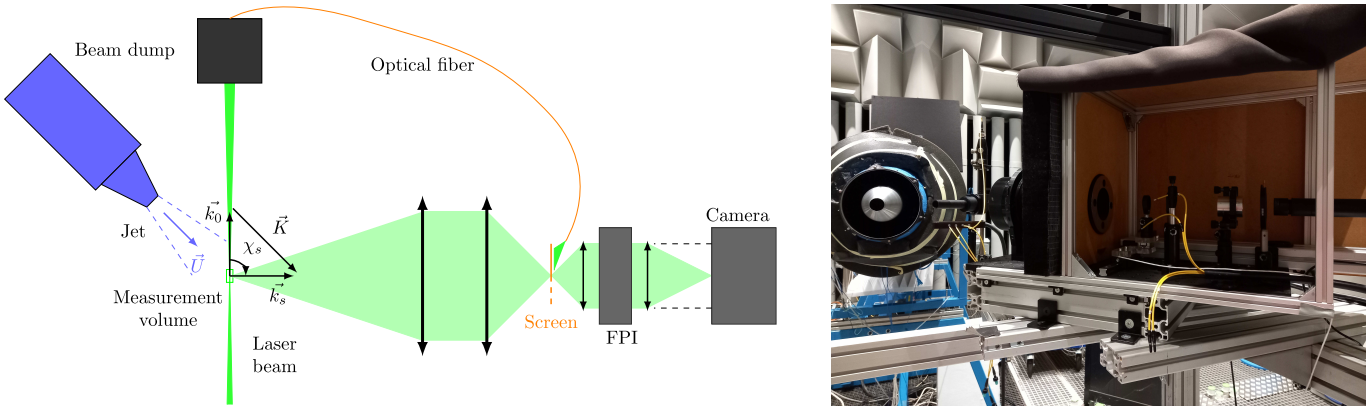

Figure 3. Experimental set-up for IRS measurements in high subsonic jets

The optical arrangement, whose principle is depicted in Figure 2, is presented in Figure 3 in its operating environment. The present experiments were conducted in the 10 m $\times$ 8 m $\times$ 8 m anechoic wind tunnel of the Center for Acoustics at École Centrale de Lyon. The wind tunnel is equipped with a high pressure compressor and a high flow rate centrifugal fan. In these experiments, the high pressure supply is connected to a convergent nozzle of exit diameter $D = 38$ mm. A secondary convergent nozzle coaxial to the primary one of diameter 227 mm is also used and fed by the fan. Each flow is equipped with on-line air filters to remove dust particles. The exit plane of this secondary nozzle is located 135 mm upstream of the exit plane of the primary one. For this study, the jet Mach number is set to $M_j = 0.9$, which corresponds to high subsonic flows of practical importance in aeronautics for instance. Far upstream the nozzle exit, the flow is heated by a set of electrical resistors, such that the jet temperature at the nozzle exit corresponds to the ambiant temperature. The heating power is adjusted to meet this criterion and the jet exhaust static temperature T_j is monitored throughout the experiment. The total temperature of the jet is thus approximately 70° C. The secondary flow is only used to shield the primary (main) jet from seeding by dust present in the anechoic room, to prevent light scattering by dust particles if they pass through the laser beam; its exit velocity U_{amb} is approximately 10 m.s^{-1}.

A continuous wave fiber laser (ALS©-GR-65) provides a 5 W laser beam, with a wavelength λ of 532 nm and a spectral bandwith of 200 kHz. The Fabry-Pérot interferometer is provided by SLS Optics Ltd., and the mirrors have a reflectivity of 89% $\pm$ 1% at the laser wavelength $\lambda_0 = 532$ nm. This corresponds to a finesse $N_R = \pi\sqrt{R}/(1-R) = 26^{+3.8}_{-1.5}$. The separation between the mirrors is $d = 20$ mm. The interferogram is imaged in the image plane, defined by the focusing lens of focal length $f_2 = 300$ mm, by a sCMOS Lavision Inc. camera whose sensor definition is 2560$\times$2160

pixels of 6.5 μm side. The exposure time of each acquired image is 0.1s, and one measurement corresponds to the acquisition of 200 images. The direction of optical axis of the whole apparatus, denoted by the wave vector k_s, makes an angle $\chi_s = 90^\circ$ with respect to direction of the laser beam, corresponding to the wave vector k_0. The angle between the jet axis and the interferometer optical axis is set to 45° such that the velocity component responsible for the frequency shift $\Delta\nu_U$ measured with the interferometer corresponds to the axial velocity component (Miles et al., 2001).

Complementary measurements are performed using CTA. A hot-wire probe (custom probe on a Dantec 55P11 basis, with wire diameter of 5 μm and length 1.25 mm) is coupled to a Dantec CTA Module 90C10 mounted in a Dantec Streamline anemometer. Time sequences of the anemometer output signal sampled at fs= 204800 Hz are stored and further processed using the CTA calibration performed *in situ* to derive mean value and standard deviation of local velocity as well as velocity distributions.

Each measurement device is mounted on a traversing system allowing a radial displacement of the measurement 'point' in the flow. For the optical measurements, it consists in a large motorized aluminium frame partly visible in Figure 3, extending under the jet flow and supporting the laser source on the right hand side of the flow and the collecting optics one the other side. The frame radial location is monitored using optical scale. The frame is free from acoustic absorbers (typically foam) provided that acoustic measurement is not carried out and that the frame is sufficiently far away from the flow to avoid any hydro-acoustic feedback loop of significant consequences on the flow development. Flow velocity profiles at the axial position located two diameters downstream of the nozzle exit are considered here.

3. Data treatment

To process Rayleigh interferograms, the physical parameters implied in the Fabry-Pérot instrument function as defined in equation (1) are needed. Moreover, it is mandatory that the parameters derived from FPI characterization still correspond to those at work as Rayleigh interferograms are recorded. Here, the laser light is used as light source for instrument function determination, thus λ corresponds to that of the laser light source. Additionally to variations in λ due to limited stability of the laser source, thermal drifts as small as a few tenth of Celsius degrees may occur and change the values of μ (dependency of the optical index to the temperature) and d (thermal dilatation). In the environment of a high speed wind tunnel, thermal exchanges between FPI casing and ambiant air in the room may be promoted by recirculating (hot) flows. Thus, one recalls here how crucial may be the variations of these parameters for the relevancy of the approach (FPI finesse N_R and f_2 are two parameters whose variation between acquisitions is neglected here). To set the orders of magnitude to be considered here, let us define the phase shift φ associated with the FPI on the optical axis, as seen in equation (1):

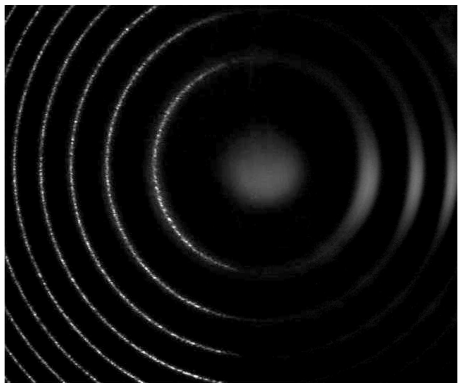

Figure 4. Experimental composite interferogram ; left part of the image: reference interferogram from laser light; right part of the image: scattered light interferogram from molecules in the probed volume

$$\varphi = \frac{2\pi\mu d}{\lambda} \tag{3}$$

$$\frac{\Delta\varphi}{\varphi} = \frac{\Delta\mu}{\mu} + \frac{\Delta d}{d} + \frac{\Delta\nu}{\nu} \tag{4}$$

For a thermal drift of 1 K, $\Delta\mu/\mu$ is around 10^{-6} (Gladston-Dale law and thermodynamics) and considerably higher than $\Delta d/d$, around 10^{-8} (manufacturer). The term $\Delta\nu/\nu$ may represent defaults in the laser source stability, which is difficult to evaluate, but could also represent the change in frequency due to Rayleigh scattering associated with a bulk motion at speed U. For $\Delta\nu/\nu$ to reach the same order of magnitude than $\Delta\mu/\mu$ (i.e. 10^{-6}), the bulk velocity U should reach 300 m.s^{-1}. Moreover, the order of magnitude for φ is 10^6; as visible in equation (1), the rest of φ modulo 2π will influence the result, so a thermal drift of 1 K will change the reference interferogram pattern (or the Rayleigh interferogram) in a great manner.

As a consequence, unless extreme care to the temperature of the medium in the FPI is taken (Clem et al., 2010), temperature stability of the FPI is the primary factor that can drastically limit the precision of flow velocity measurement. The choice has been made here to design a specific interferometer arrangement, in which laser light entering an optical fiber at the rear end of the beam dump is used to en-light a screen placed on part of the field of view of the FPI arrangement, as depicted in Figure 3. This allows to form on the camera sensor a composite image, for half made of the interferogram obtained for the FPI submitted to scattered light from the probed volume within the jet, and for half made of interferogram obtained for the FPI submitted to (reference) laser light. This way, each composite image, as that depicted in Figure 4, can be analyzed together with a simultaneous reference ; in the case this reference would change from one image to another due to thermal drift, the analysis of the scattered light would be performed with an embedded simultaneously-acquired reference.

After having split the composite interferogram into two parts, one proceeds with their analysis

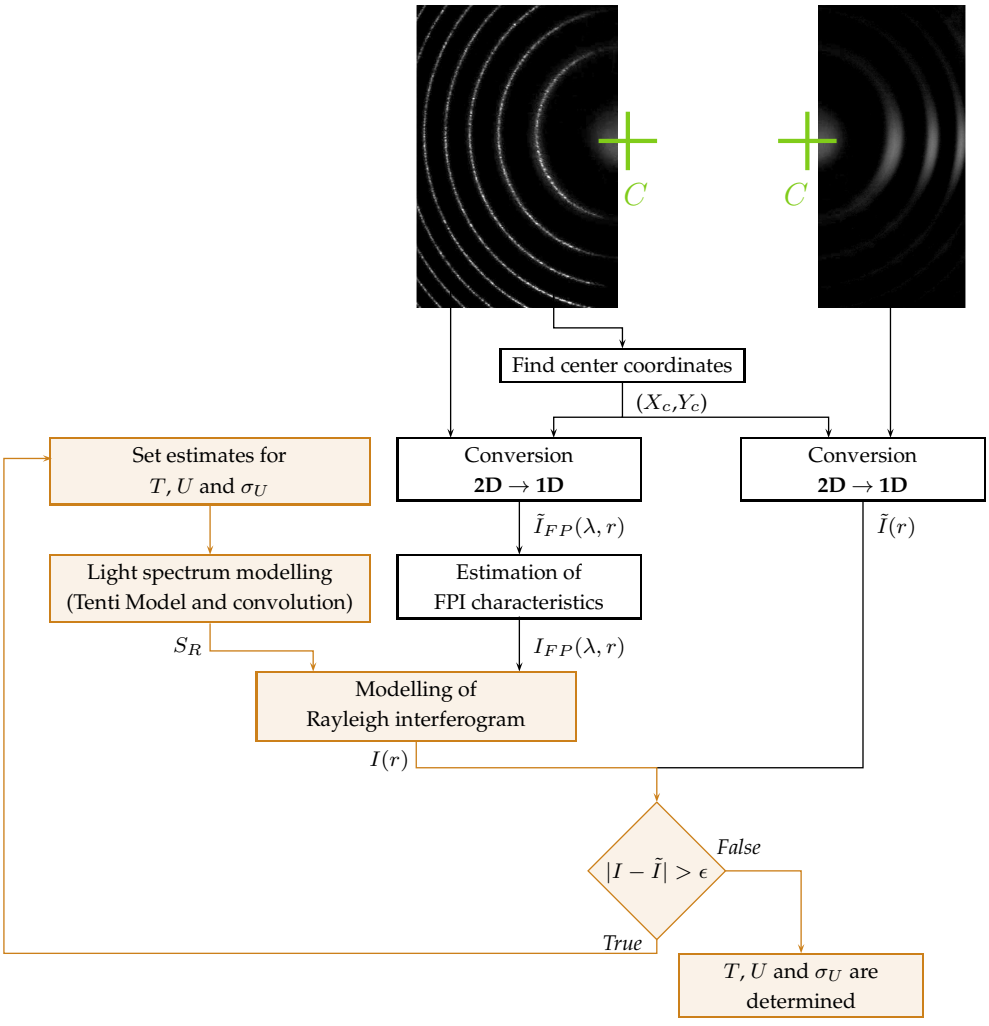

Figure 5. Diagram of the procedure for determining the values of temperature T, velocity U and standard deviation of the velocity σ_U on the basis of a composite interferogram.

following the procedure summarized in Figure 5. After determining the center of the reference interferogram (left part of the composite interferogram), this image is converted into a 1D-data set which provides an estimate of the Fabry-Pérot instrument function. This estimate is noted $\tilde{I}_{FP}(\lambda, r)$ and is used as input to determine the FPI characteristics. After this step, a modeled instrument function $I_{FP}(\lambda, r)$ that implies the Fabry-Pérot characteristics determined above, is built. Similarly, the right part of the composite image is also converted in a 1D-data set, using the coordinates of the interferogram center as determined using the reference interferogram. The different steps of the procedure described so far are detailed in Kurek (2024) and are beyond the scope of the present study, which mainly focuses on the complementary approach highlighted by the light-red boxes in the diagram of Figure 5.

One first build a non-dimensional spectrum of the light scattered by molecules of a flow of temperature T, velocity U and standard deviation of the velocity σ_U. To do so, one prescribes given (initial) values for these three parameters, and assumes that the velocity distribution at the location of the probe volume is Gaussian. One samples this distribution over 10 values. For each sample, the scattered light spectrum is estimated using Tenti S6 model (Tenti et al., 1974), and weighted by the value of the Gaussian distribution at the sample value. The scattered light spectrum S_R is consequently obtained by summing these different estimates. A simple sum is allowed here because we want to represent the accumulation of light over the camera sensor during an exposure time which is long with respect to the turbulence time scales: no interference is at play here. The convolution between the non-dimensional spectrum S_R and the modeled instrument function $I_{FP}(\lambda, r)$ is computed, following Equation (2), and this result is compared to the 1D-data set extracted from Rayleigh interferogram. The comparison consists in the evaluation in the least squares sense of the difference between the two functions I_{FP} and $\tilde{I}_{FP}$ around the first peak (thus the first circle arc in the Rayleigh interferogram). If the match is good enough, the values of T, U and σ_U are recorded and serve as estimates of the flow temperature, mean axial velocity and standard deviation of the axial velocity at the probe volume location. Otherwise, a new set of values is tested. In practice, the results are obtained by using a non-linear least squares minimization algorithm (*lsqnonlin* with Levenberg-Marquardt algorithm in Matlab). In the interferograms analysis procedure, the temperature T is set and not retrieved from measurements; indeed, either velocity fluctuations and temperature contribute to the shape of the intensity response $I(r)$. The temperature may influence $I(r)$ through its mean value, at play in $S_R(\lambda)$ (Equation 2) but also through its fluctuations, as for the velocity. In the case of isothermal jets, this last effect is supposed to be small with respect to the effects of the mean temperature and the velocity fluctuations. Two complementary approaches are thus considered in the following:

a- The jet temperature is considered homogeneous and equal to the ambiant temperature T_∞: this corresponds to neglect compressible effects in the turbulent jet shear layer, that contribute to increase the local temperature,

b- The isothermal jet temperature distribution is deduced from the Crocco-Busemann relation, taking into account compressibility effects (Pineau & Bogey, 2019):

$$\frac{T}{T_\infty} = 1 + \frac{\gamma - 1}{2} M_j^2 \frac{U}{U_j} \left(1 - \frac{U}{U_j}\right) \tag{5}$$

where γ is the polytropic constant for air, M_j is the jet Mach number and U_j the related velocity.

4. Results

The $M_j = 0.9$ isothermal jet axial velocity profiles measured at the axial location $x_0/D = 2$, with D the nozzle diameter, are considered now. One compares in Figure 6(a) the measurements of the time averaged velocity obtained by traversing the hot wire probe along the radial direction R to those derived from the analysis of Rayleigh interferograms described in section 3. The results are given as a function of η, corresponding to the radial coordinate R made dimensionless by the momentum thickness of the shear-layer δ_θ at the axial location $x_0/D = 2$, and centered on the radial coordinate $R_{1/2}$ for which the local velocity is equal to half U_j. A very good match is obtained between the two sets of results. The estimate of the temperature change in the jet due to compressible effects (Equation (5)) is derived from the hot-wire velocity measurements and plotted in Figure 6(b). The maximum increase temperature is expected to be around 12K, at the location of maximum shear ($\eta = 0$).

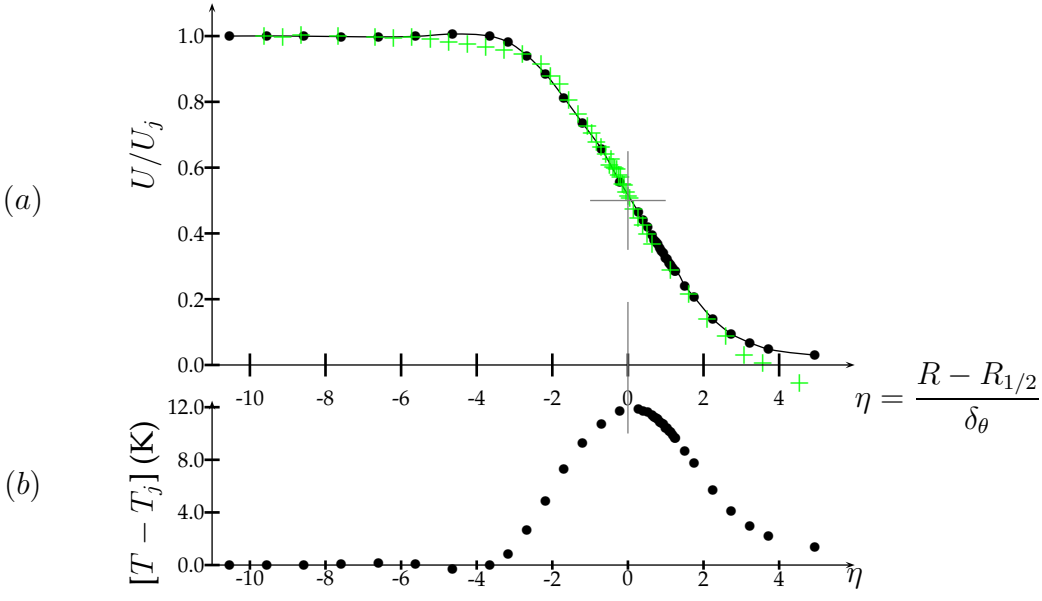

Figure 6. Velocity profiles in a $M_j = U_j/c_0 = 0.9$ jet across the section located $2D$ downstream of the nozzle exit: (a) Normalized mean axial velocity (b) Variation of static temperature within the jet estimated using Equation (5) and hot wire measurements of the mean axial velocity. (•): hot wire measurements; (+): IRS measurements

The estimation of the standard deviation for the axial velocity component is presented in Figure 7. Considering first the hot wire results, one retrieves that the velocity fluctuations are, as expected, small in the potential region of the jet, in particular near the jet axis, and increase up to a maximum located at the center of the jet shear layer. This maximum corresponds to 13% of U_j, in good agreement with previous measurements on jet flows in this facility (Castelain, 2006). For the results derived from the Rayleigh interferogram analysis, two data-sets are examined following the approaches presented in section 3. If the temperature is considered constant over the radial profile, the estimated velocity fluctuations reach 23% of the jet velocity. Besides, this maximum in the velocity fluctuations profile is located slightly on the outer side of the jet shear layer, which is not consistent with the physics at work. Nevertheless, the low level of turbulence in the jet core is well retrieved, and a clear difference between the results obtained in the jet shear layer and in the jet core appears. For the approach with temperature estimation inside the jet, whose radial evolution in presented in Figure 6(b), the temperature is set, prior to the analysis of each Rayleigh interferogram, to the local value estimated from Equation (5). Even if the trend in the velocity fluctuations profile obtained this way differs from the reference one (hot-wire measurement), with a clear under-estimation of the turbulence intensity in the inner-part of the shear layer and an over-estimation in its outer region, one may remark that the turbulence intensity level at the jet shear layer center ($\eta = 0$) is in very good agreement with hot-wire data, as well as its level in the jet core. It appears clearly that the value assigned to the local mean temperature as input for the Rayleigh interferogram analysis plays a crucial role in the estimation of turbulence level. Indeed, for example for $\eta = -2$, the temperature correction brought by Equation (5) is 5K; this small temperature correction is responsible for a significant change in the velocity fluctuations estimate, from 10% to nearly 0.1%. For instance, the overestimation of velocity fluctuations of the outer side of the jet shear layer is attributed to a slight temperature difference between the jet temperature and the ambiant temperature (of around 3K). One should also point out that temperature fluctuations, whose effects were neglected here, may also have an effect on the scattered light spectrum; this effect is supposed to be moderate in the case of the isothermal jet considered here, but its order of magnitude would have to be confirmed. Additionally, if the velocity distribution can be approximated to a Gaussian distribution at the jet shear layer center ($\eta = 0$), the relevancy of this assumption is known to be less effective apart from this location (Anselmet et al., 1984). A further study may thus focus on the effects of these assumptions on the estimation of velocity fluctuations.

5. Conclusions

Measurements of velocity fluctuations level inside a compressible isothermal jet obtained by Interferometric Rayleigh Scattering have been derived from long-time exposure interferograms. This approach is motivated by the development of a dedicated optical arrangement that allows for capturing simultaneously the reference interferogram in one hand and the Rayleigh interferogram

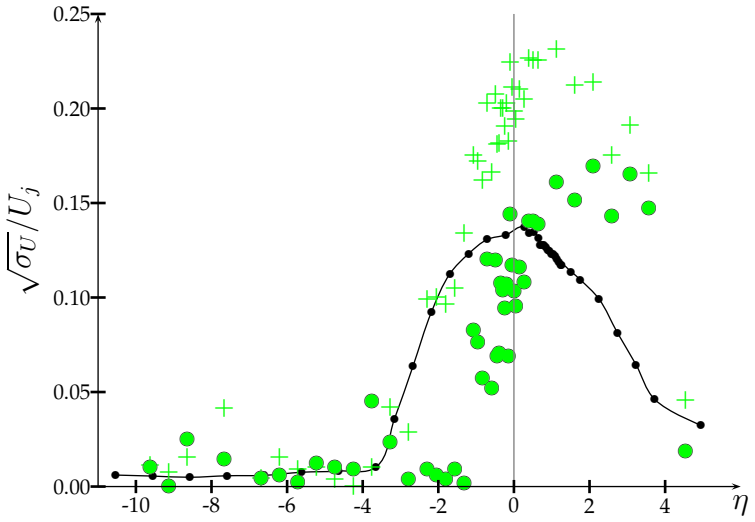

Figure 7. Profiles of velocity fluctuations in a $M_j = U_j/c_0 = 0.9$ jet, across the section located $2D$ downstream of the nozzle exit. (•): hot wire measurements; (+): IRS measurements with constant temperature assumption; (•): IRS measurements with modeled temperature variation using Equation (5)

from scattering molecules within the jet in the other hand. Owing to the low efficiency of the Rayleigh scattering process, capturing Rayleigh interferograms with long-time exposure is relevant to increase the signal-to-noise ratio. Doing so, a blurring of the circular fringes arises on the Rayleigh interferogram because of the unsteadiness of the physical parameters at play concerning the light scattering molecules, and in particular velocity fluctuations. This effect is modeled here by considering a Gaussian model of velocity fluctuations whose standard deviation is taken as an input parameter to build a scattered light spectrum model which includes the contributions of the different molecules along time, at a given position in the jet, that will act as light source for the Rayleigh interferogram. The output of a minimization process between the modeled interferogram and the measured one provides an estimate of the velocity fluctuations. This method is shown here to provide a very good estimate of the velocity fluctuations, as compared to that derived from hot-wire measurements in the same flow. Its sensitivity to input parameters, and in particular static temperature, is pointed out. Nevertheless, it is remarkable to achieve turbulence level estimation by a method which does not require any in-flow calibration nor flow length- or time-scale measurements, and can operate at time scales several order of magnitude higher than the flow characteristics time scales.

Acknowledgements

The authors acknowledge the financial support by Labex CeLyA of Université de Lyon, operated by the French National Research Agency grant number ANR10-LABX-0060/ANR-11-IDEX-0007. This work was performed within the framework of the industrial chair ARENA (ANR-18-CHIN-0004-01) co-financed by Safran Aircraft Engines and the French National Research Agency (ANR).

References

Anselmet, F., Gagne, Y., Hopfinger, E. J., & Antonia, R. A. (1984). High-order velocity structure functions in turbulent shear flows. *J.Fluid Mech.*, *140*, 63–89.

Castelain, T. (2006). *Contrôle de jet par microjets impactants. mesure de bruit rayonné et analyse aérodynamique,* (PhD thesis 2006-33). Ecole Centrale de Lyon.

Clem, M. M., Mielke-Fagan, A. F., & Elam, K. A. (2010). Study of fabry-perot etalon stability and tuning for spectroscopic rayleigh scattering. In *48th aiaa aerospace sciences meeting including the new horizons forum and aerospace exposition.*

Cutler, A. D., Rein, K., Roy, S., Danehy, P. M., & Jiang, N. (2020). 100-khz interferometric rayleigh scattering for multi-parameter flow measurements. *Optics Express*, *28*(3), 3025–3025.

Estevadeordal, J., Jiang, N., Cutler, A. D., Felver, J. J., Slipchenko, M. N., Danehy, P. M., ... Roy, S. (2018). High-repetition-rate interferometric rayleigh scattering for flow-velocity measurements. *Applied Physics B: Lasers and Optics*, *124*(3), 1–6.

Kurek, I. (2024). *Mesures de vitesse, température et masse volumique par diffusion rayleigh et étude de l'effet de vol sur les ondes guidées dans des jets subsoniques* (PhD thesis 2024ECDL0001). Ecole Centrale de Lyon.

Mercier, B., Castelain, T., Jondeau, E., & Bailly, C. (2018). Fluctuations measurement by rayleigh scattering using a single photomultiplier. *AIAA Journal*, *56*(4), 1310–1316.

Mielke, A., Seasholtz, R., Elam, K., & Panda, J. (2005). Time-average measurement of velocity, density, temperature, and turbulence velocity fluctuations using rayleigh and mie scattering. *Experiments in Fluids*, *39*, 441–454.

Miles, R. B., Lempert, W. R., & Forkey, J. N. (2001). Laser rayleigh scattering. *Measurement Science and Technology*, *12*(5), R33.

Panda, J. (2020). Spectrally-resolved rayleigh scattering to measure velocity, temperature, density, and density fluctuations in high-speed flows. *Experiments in Fluids*, *61*(3), 1–16.

Panda, J., & Seasholtz, R. (1999). Velocity and temperature measurement in supersonic free jets using spectrally resolved rayleigh scattering. In *37th aerospace sciences meeting and exhibit, american institute of aeronautics and astronautics, reston, virigina, 1999, pp. aiaa 99–0296.*

Pineau, P., & Bogey, C. (2019). Temperature effects on the generation of steepened waves by supersonic temporal round jets. In *25th aiaa/ceas aeroacoustics conference.*

Seasholtz, R. G., Buggele, A. E., & Reeder, M. F. (1997). Flow measurements based on rayleigh scattering and fabry-perot interferometer. *Optics and Lasers in Engineering*, *27*(6), 543–570.

Tenti, G., Boley, C. D., & Desai, R. C. (1974). On the kinetic model description of rayleigh–brillouin scattering from molecular gases. *Canadian Journal of Physics*, *52*(4), 285-290.